Published in final edited form as:

Mater Sci Eng C Mater Biol Appl. 2016 April 01; 61: 437–448. doi:10.1016/j.msec.2015.12.090.

Culturing on decellularized extracellular matrix enhances antioxidant properties of human umbilical cord-derived mesenchymal stem cells

Xiaozhen Liu[a,1], **Long Zhou**[b,c,1], **Xi Chen**[b,c], **Tao Liu**[c], **Guoqing Pan**[b,c], **Wenguo Cui**[b,c], **Mao Li**[b,c], **Zong-Ping Luo**[b,c], **Ming Pei**[d], **Huilin Yang**[b,c], **Yihong Gong**[a,*], **Fan He**[b,c,**]

[a]School of Engineering, Sun Yat-sen University, Guangzhou 510006, China

[b]Orthopaedic Institute, Soochow University, Suzhou 215007, China

[c]Department of Orthopeadics, The First Affiliated Hospital of Soochow University, Suzhou 215006, China

[d]Stem Cell and Tissue Engineering Laboratory, Department of Orthopaedics, West Virginia University, Morgantown, WV 26506, USA

Abstract

Human umbilical cord-derived mesenchymal stem cells (UC-MSCs) have attracted great interest in clinical application because of their regenerative potential and their lack of ethical issues. Our previous studies showed that decellularized cell-deposited extracellular matrix (ECM) provided an *in vivo*-mimicking microenvironment for MSCs and facilitated *in vitro* cell expansion. This study was conducted to analyze the cellular response of UC-MSCs when culturing on the ECM, including reactive oxygen species (ROS), intracellular antioxidative enzymes, and the resistance to exogenous oxidative stress. After decellularization, the architecture of cell-deposited ECM was characterized as nanofibrous, collagen fibrils and the matrix components were identified as type I and III collagens, fibronectin, and laminin. Compared to tissue culture polystyrene (TCPS) plates, culturing on ECM yielded a 2-fold increase of UC-MSC proliferation and improved the percentage of cells in the S phase by 2.4-fold. The levels of intracellular ROS and hydrogen peroxide (H_2O_2) in ECM-cultured cells were reduced by 41.7% and 82.9%, respectively. More importantly, ECM-cultured UC-MSCs showed enhanced expression and activity of intracellular antioxidative enzymes such as superoxide dismutase and catalase, up-regulated expression of silent information regulator type 1, and suppressed phosphorylation of p38 mitogen-activated protein kinase. Furthermore, a continuous treatment with exogenous 100 μM H_2O_2 dramatically inhibited osteogenic differentiation of UC-MSCs cultured on TCPS, but culturing on ECM retained the differentiation capacity for matrix mineralization and osteoblast-specific marker gene

*Corresponding Authors: Yihong Gong, Ph.D., School of Engineering, Sun Yat-sen University, No.132 East Waihuan Road, Guangzhou Higher Education Mega Center, Guangzhou 510006, Guangdong, China. Telephone: +86-20-39332146; Fax: +86-20-39332146; gongyih@mail.sysu.edu.cn. **Fan He, Ph.D., Orthopaedic Institute, Soochow University, No.708 Renmin Road, Suzhou 215007, Jiangsu, China. Telephone: +86-512-67781420; Fax: +86-512-67781165; fanhe@suda.edu.cn.
[1]These authors contributed equally to this work.

Conflicts of interest

The authors declare no conflicts of interest.

expression. Collectively, by providing sufficient cell amounts and enhancing antioxidant capacity, decellularized ECM can be a promising cell culture platform for *in vitro* expansion of UC-MSCs.

Keywords

extracellular matrix; mesenchymal stem cells; antioxidative enzymes; reactive oxygen species; osteogenesis

1. Introduction

Mesenchymal stem cells (MSCs), also referred to adult stem cells, represent a cell population that is responsible for new tissue growth and tissue repair. MSCs have attracted great interest because of their regenerative potential and immunomodulatory properties. MSCs were identified first in bone marrow stroma [1] and can be isolated from various adult organs or tissues, such as adipose tissue, synovial membrane, periosteum, and amniotic fluid [2]. Currently, human umbilical cord-derived mesenchymal stem cells (UC-MSCs), in particular from Wharton's jelly tissue, are considered a promising candidate for cell therapy and regenerative medicine [3]. Since the human umbilical cord is an extraembryonic tissue, UC-MSCs are supposed to feature characteristics of both embryonic and adult stem cells [4]. Also, umbilical cords, which are discarded as waste after delivery, can be obtained with a harmless and safe procedure, so obtaining UC-MSCs has not raised any ethical problems. Recent studies have proven that UC-MSCs share similar cell surface markers (such as CD29, CD44, CD90, CD105, and vimentin) [5] with MSCs derived from other sources, maintain multilineage differentiation potentials (such as the ability to differentiate into osteoblasts, chondrocytes, adipocytes, neurons, and hepatocytes) [6], and more importantly, show a faster capacity for self-renewal than MSCs derived from bone marrow [7].

Although MSCs have attracted much attention owing to their therapeutic uses for regenerative medicine, *in vitro* expansion and *in vivo* transplantation of MSCs expose them to considerable oxidative stress, resulting from excessive levels of reactive oxygen species (ROS), such as hydrogen peroxide (H_2O_2), the hydroxyl radical, and superoxide anion radicals. An increased level of intracellular H_2O_2 was measured during long-term *in vitro* culturing of MSCs and was considered to be responsible for the initiation of cellular senescence and inhibition of proliferation [8]. Abnormal levels of ROS, generated endogenously by local chondrocytes or exogenously by neutrophils and macrophages, have been implicated in osteoarthritis [9] and rheumatoid arthritis [10], compromising the regenerative potential of MSCs. Our previous studies demonstrated that over-accumulation of ROS was caused by exposure to inflammatory cytokines, resulting in suppression of cell proliferation and multi-lineage differentiation [11, 12].

The balance between generation and elimination of ROS is crucial for cell survival, proliferation, and lineage-specific differentiation. Superoxide dismutase (SOD), including the isoenzymes that contain copper, zinc (SOD1 and SOD2) and manganese (SOD2) [13], protects MSCs from ROS by catalyzing the superoxide anion to hydrogen peroxide. Choi et al. reported that an intracellular delivery system for SOD1 by a cell-penetrating peptide restored cell proliferation and osteogenic differentiation in human dental pulp-derived

MSCs, which were inhibited by oxidative stress [14]. On the other hand, inhibition of SOD2 caused suppressed chondrogenic differentiation of human synovium-derived MSCs and increased expression of matrix metalloproteinases [12]. Furthermore, H_2O_2 produced by SOD enzymes is neutralized by catalase and glutathione peroxidases (GPxs). A number of previous studies demonstrated that enhancing catalase activity contributed to MSC resistance to H_2O_2-induced apoptosis [15] and selenium supplementation reduced cell damage by restoring GPx activity [16].

Our previous work suggested that, after decellularization, MSC-deposited extracellular matrix (ECM) can be used as a novel *in vitro* culture system to facilitate MSC expansion [17] and to direct MSCs towards lineage-specific commitment [18]. This decellularized ECM is not only considered to mimic *in vivo* extracellular microenvironment for stem cells, but it also modulates the biological actions of growth factors [19] and hormones [20]. This culturing method, using decellularized ECM, prevents replicative senescence and enhances redifferentiation in terminally differentiated cells, such as chondrocytes [21] and nucleus pulposus cells [22]. A recent finding indicated that decellularized ECM improved the resistance of MSCs to H_2O_2-induced oxidative stress and cell cycle arrest [23]. However, little is known about the intracellular antioxidative response of UC-MSCs when culturing on the decellularized ECM. In this study, we hypothesized that UC-MSCs cultured on decellularized ECM would acquire enhanced antioxidant properties and exhibit an improved resistance to oxidative stress. To test this hypothesis, MSC-deposited ECM was decellularized and characterized, and UC-MSCs were cultured on decellularized ECM and ordinary tissue culture polystyrene (TCPS). Cell proliferation, intracellular levels of ROS and H_2O_2, and expression and activity of antioxidative enzymes were analyzed. We further examined the cellular response of UC-MSCs on ECM by exposure to exogenously H_2O_2-induced oxidative stress.

2. Materials and Methods

2.1 Cell culture of UC-MSCs

Human UC-MSCs were purchased from the American Type Culture Collection (ATCC; Manassas, VA, USA) and cultured in growth medium [alpha minimum essential medium (α-MEM) supplemented with 10% fetal bovine serum (FBS; Thermo Fisher Scientific, Waltham, MA, USA), 100 U/mL penicillin, and 100 μg/mL streptomycin (Invitrogen, Carlsbad, CA, USA)] at 37°C with 5% CO_2 in 175 cm^2 cell culture flasks (Thermo Fisher). The medium was changed every 3 days. Cells were dissociated by 0.25% trypsin-EDTA (Invitrogen) and reseeded into multi-well plates for the next stage of the experiments.

2.2 Preparation of decellularized ECM deposited by UC-MSCs

TCPS plates were treated with 0.2% gelatin (Sigma-Aldrich, St. Louis, MO, USA) for 1 h at 37°C, followed by 1% glutaraldehyde (Sigma-Aldrich) and 1 M ethanolamine (Sigma-Aldrich) for 30 min at room temperature. On pretreated plates, the UC-MSCs were cultured in growth medium until reaching 90% confluence, and then 100 μM L-ascorbic acid was added for an additional culture period of eight days. To obtain cell-free ECM, cultured cells were incubated in extraction buffer [0.5% Triton X-100 and 20 mM NH_4OH (Sigma-

Aldrich) in phosphate buffered saline (PBS), pH = 7.4] for 5 min at 37°C, and subsequently treated with 100 U/mL DNase I (Sigma-Aldrich) for 1 h at 37°C. Decellularized ECM was washed with PBS three times to remove the residual DNase and then was stored under sterile conditions at 4°C.

2.3 Scanning electron microscopy (SEM) analysis

Decellularized ECM was fixed in 2.5% glutaraldehyde and dehydrated in increasing concentrations of ethanol (50%, 75%, 80%, 95%, and 100%). The morphology of decellularized ECM was analyzed by a scanning electron microscope (S-520; Hitachi High-Technologies, Tokyo, Japan).

2.4 Immunofluorescence staining

Decellularized ECM was fixed in 4% paraformaldehyde (Sigma-Aldrich), blocked in 1% bovine serum albumin (BSA), and incubated in appropriately diluted primary antibodies against type I collagen, type III collagen, fibronectin, and laminin (Abcam, Cambridge, MA, USA). After rinsing with PBS, ECM was incubated in diluted secondary antibodies (Alexa Fluor® 488 donkey anti-mouse IgG, Invitrogen). Fluorescence images were obtained with an Olympus IX51 microscope (Olympus Corporation, Tokyo, Japan).

2.5 Cell viability stain and cell proliferation assay

UC-MSCs were seeded on TCPS and ECM-treated plates separately at the indicated cell density at 37°C in 5% CO_2. Cell viability was assessed by fluorescein diacetate (FDA; Sigma-Aldrich) staining. Cells were washed with PBS and incubated in 5 μg/mL FDA solution at 37°C for 10 min. After washing with PBS, fluorescence images were captured with an Olympus IX51 microscope.

Cell proliferation was evaluated by a DNA assay, which represented a proxy for the number of cells, using the Quant-iT™ PicoGreen® dsDNA Assay Kit (Invitrogen). Two hundred μL of papain lysis buffer (125 μg/mL in PBS; Sigma-Aldrich) was added to each well, and the cells were lysed at 60°C for 4 h. Equal quantities of lysates and reagents were added to a 96-well plate and resulting samples were incubated in the dark for 5 min. Fluorescence of the samples was measured on a SynergyMx multi-mode microplate reader (BioTek, Winooski, VT, USA) at 485/520 nm (excitation/emission), alongside a standard curve.

2.6 Cell cycle analysis

Cell cycle distribution analysis was assessed by propidium iodide (PI) staining. Adherent cells were dissociated by trypsinization and fixed in 70% ethanol at 4°C for 24 h. After washing with PBS, samples were treated with 50 μg/mL PI (Sigma-Aldrich) and 50 μg/mL RNase A (Sigma-Aldrich) at 37°C for 30 min. Samples were analyzed using a Cytomics FC500 Flow Cytometer (Beckman-Coulter, Brea, CA, USA) and at least 5,000 cells were collected per sample. Data were analyzed using the MultiCycle AV DNA analysis software (Phoenix Flow Systems, San Diego, CA, USA).

2.7 Intracellular reactive oxygen species (ROS) accumulation

Intracellular levels of ROS were quantified by the DCF-DA fluorescence method. 2×10^5 cells were incubated in 10 μM 2′,7′-dichlorofluorescein diacetate (DCF-DA) at 37°C for 10 min. The fluorescence intensity was measured using a Cytomics FC500 Flow Cytometer and 10,000 events from each cell sample were analyzed using the WinMDI (Windows Multiple Document Interface for Flow Cytometry) 2.9 software.

2.8 Intracellular hydrogen peroxide (H_2O_2) accumulation

Intracellular levels of H_2O_2 were detected with the Amplex® Red Hydrogen Peroxide Assay Kit (Invitrogen) according to the manufacturer's instructions. Cells cultured on TCPS and on ECM were suspended in cell lysis solution and cellular extracts were collected. Each lysate was mixed with the reagent from the kit and incubated for 30 min. Fluorescence was measured using a fluorescence microplate reader (BioTek) at 530/590 nm (excitation/emission).

2.9 Superoxide dismutase activity assay

Total SOD activity was analyzed by the SOD assay kit (Beyotime Institute of Biotechnology, Haimen, China) according to the manufacturer's instructions. Cells cultured on TCPS and on ECM were suspended in cell lysis solution and protein amount was quantified with the BCA protein assay kit (Beyotime). Each lysate was mixed with reagent from the kit and incubated at 37°C for 20 min. Absorbance at 450 nm was measured using a microplate reader (BioTek).

2.10 Catalase activity assay

Catalase activity was measured by a commercially available assay kit (Sigma-Aldrich) according to the manufacturer’s instructions. Protein samples were prepared by lysis and total lysate proteins were quantified with a BCA protein assay kit (Beyotime). Each lysate was mixed with colorimetric assay substrate solution from the kit and incubated at room temperature for 15 min. Absorbance at 520 nm was measured using a microplate reader (BioTek), alongside a standard curve.

2.11 Osteogenic differentiation and Alizarin Red S staining

To induce UC-MSCs into osteogenic lineage commitment, cells were cultured in osteogenic differentiation medium [Dulbecco’s modified Eagle medium (DMEM; Thermo Fisher) was supplemented with 10% FBS, 100 U/mL penicillin, 100 μg/mL streptomycin, 50 μg/mL L-ascorbic acid, 100 nM dexamethasone, and 10 mM β-glycerol phosphate (Sigma-Aldrich)] for 21 days. To investigate the protective effects of culturing on ECM on MSC osteogenesis, exogenous 100 μM H_2O_2 was added to the osteogenic differentiation medium to create an oxidative microenvironment. The differentiation medium was changed every 3 days.

Mineralization of the matrix was determined by Alizarin Red S staining. Cells were fixed in 4% paraformaldehyde and incubated in 1% Alizarin Red S solution (pH = 4.3; Sigma-Aldrich) for 15 min. Images of calcium deposition were captured using an Olympus IX51 microscope. To quantify the calcified matrix, 200 μL/well of 1% hydrochloric acid

(Sigma-Aldrich) was added and absorbance was measured at 420 nm using a microplate spectrophotometer (BioTek).

2.12 Total RNA extraction and real-time reverse transcription-polymerase chain reaction (real-time RT-PCR)

Total RNA was extracted using TRIzol® reagent (Sigma-Aldrich); 1 μg of total RNA was reverse-transcribed using the RevertAid First Strand cDNA Synthesis Kit (Thermo Fisher). To quantify mRNA expression, an amount of cDNA equivalent to 50 ng of total RNA was amplified by real-time PCR using the iTap™ Universal SYBR® Green Supermix kit (Bio-Rad, Hercules, CA, USA). Transcript levels of antioxidative enzymes, including *SOD1*, *SOD2*, *CAT* (catalase), and *GPX1*, *SIRT1*, and osteogenic marker genes, including *COL1A1* (type I collagen α1), *SPP1* (secreted phosphoprotein 1 or osteopontin), *ALP* (alkaline phosphatase), *RUNX2* (runt-related transcription factor 2), *BGLAP* (bone gamma carboxyglutamate protein or osteocalcin), and *SP7* (Sp7 transcription factor 7 or osterix) were evaluated. *GAPDH* (glyceraldehyde-3-phosphate dehydrogenase) served as an internal standard. The primer sequences were listed in Table 1. Real-time PCR was performed on a CFX96™ Real-Time PCR System (Bio-Rad) following the manufacturer's protocol. Relative transcript levels were calculated as $\chi = 2^{-\Delta\Delta Ct}$, in which $\Delta\Delta Ct = \Delta E - \Delta C$, $\Delta E = Ct_{exp} - Ct_{GAPDH}$, and $\Delta C = Ct_{ct1} - Ct_{GAPDH}$.

2.13 Western blot analysis

Cells were lysed in ice-cold cell lysis buffer (Beyotime) containing protease inhibitors (Thermo Fisher) and the protein concentration in cell extracts was quantified using the BCA protein assay kit (Beyotime). Equal amounts of protein from each extract were denatured and separated in a 10% polyacrylamide gel (Beyotime), and then transferred by electrophoresis onto a nitrocellulose membrane (Thermo Fisher). The membrane was incubated in diluted primary antibodies against SIRT1, p38, phosphor p38 (T180 + Y182), SOD1, SOD2, catalase, GPx1, and α-tubulin (Abcam) at 4°C overnight. Membranes were then incubated in horseradish peroxidase-conjugated anti-mouse or anti-rabbit secondary antibodies. The membranes were developed using SuperSignal West Pico Substrate and CL-XPosure Film (Thermo Fisher). The intensity of bands was quantified using ImageJ software (National Institutes of Health, Bethesda, MD, USA).

2.14 Statistical analysis

All data were expressed as the mean ± standard error (S.E.). Statistical differences between the two groups were determined by one-way analysis of variance (ANOVA) followed by Student's unpaired *t*-test, using the SPSS 13.0 statistical software (SPSS Inc, Chicago, IL, USA). Significance was indicated by a *p*-value of < 0.05 (*) or < 0.01 (**)

3. Results

3.1 Evaluation of native ECM deposited by UC-MSCs

In order to produce a native ECM, pretreatments with gelatin, glutaraldehyde, and ethanolamine were adopted to enhance the adhesive force between ECM and the ordinary culture surface. Subsequently, exogenous 100 μM L-ascorbic acid was supplemented to

stimulate ECM production for an additional culture period of 8 days. Cell-deposited ECM was decellularized by treatments with Triton X-100, NH_4OH, and DNase I to remove the originally ECM-producing cells and DNA remnants.

After decellularization, the native ECM appeared as a white membrane-like material with a fibrous structure (Figure 1(A)). The SEM image taken at 40000× showed that the architecture of the decellularized ECM was net-like; the lattices were composed of small bundles of nanofibrous, collagen fibrils (Figure 1(B)). Four known matrix proteins (type I collagen, type III collagen, fibronectin, and laminin) were identified within the structure of decellularized ECM using immunofluorescence staining (Figure 1(C)).

3.2 MSC proliferation on decellularized ECM

To investigate how culturing on ECM affected the proliferative potential of UC-MSCs, UC-MSCs were seeded at a series of initial cell densities, and DNA assays were conducted at different time points. First, UC-MSCs were seeded on TCPS and ECM-coated surfaces at the cell density of 1,000 cells/cm^2 and cultured for 7 days. On days 3, 5, and 7, UC-MSCs on ECM yielded 50.0 ± 4.5 ng, 187.4 ± 7.4 ng, and 280.9 ± 8.7 ng of DNA content per well, respectively, compared to the DNA content of culturing UC-MSCs on TCPS at 33.5 ± 8.8 ng, 77.2 ± 6.8 ng, and 161.5 ± 6.9 ng per well (Figure 2(A)). Furthermore, UC-MSCs were seeded on TCPS and ECM at the cell densities 100, 1,000, and 5,000 cells/cm^2 and cultured for 5 days. DNA assay results revealed that culturing on ECM improved cell growth by 78.1% at a density of 100 cells/cm^2, 2.2-fold at a density of 1,000 cells/cm^2, and 2.3-fold at a density of 5,000 cells/cm^2, compared to culturing on TCPS (Figure 2(B)). Consistent with Fig. 2A, FDA staining results confirmed that culturing on ECM increased cell number and UC-MSCs on decellularized ECM exhibited a small, spindle-like cell shape (Figure 2(C)). We used flow cytometry to analyze the cell cycle distribution (Figure 2(D)). Cells cultured on TCPS exhibited a significantly higher proportion in the G0/G1 phase (78.5 ± 3.7% on TCPS vs. 65.2 ± 2.1% on ECM). In contrast, culturing on ECM increased the entry of proliferating cells into the S phase (10.4 ± 2.1% on TCPS vs. 25.1 ± 1.5% on ECM). UC-MSCs in the G2/M phase showed similar proportions in the TCPS- and ECM-cultured groups.

3.3 Intracellular ROS and related proteins in ECM-cultured UC-MSCs

We next examined the effect of culturing UC-MSCs on ECM on intracellular ROS and related protein expression. Flow cytometry analysis of DCF fluorescence intensity showed that ROS accumulation in ECM-cultured UC-MSCs was 41.7 ± 1.0% lower than that of the TCPS-cultured cells (Figure 3(A)). Analysis of intracellular H_2O_2, labeled by Amplex® Red dye, revealed that culturing on ECM induced an 82.9 ± 2.6% reduction compared with cells cultured on the TCPS surface (Figure 3(B)). Furthermore, we detected mRNA and protein levels of SIRT1, which is a nicotinamide adenine dinucleotide-dependent deacetylase with anti-aging activities [24]. Culturing of UC-MSCs on ECM resulted in a 2-fold increase of *SIRT1* mRNA expression (Figure 3(C)) and a 41% increase of protein expression (Figure 3(D)) compared to the TCPS-cultured cells. In addition, we measured activation of p38 mitogen activated protein kinase (MAPK), which is involved in replicative senescence in MSCs during *in vitro* expansion [25]. Western blot analysis revealed that phosphorylation

(p-) level of p38 in ECM-cultured cells was 56.3% lower than that of the TCPS-cultured cells, but the difference of total p38 protein expression between the two groups was not significant (Figure 3(E)).

3.4 Effects of culturing UC-MSCs on ECM on the expression and activity of SOD

To illustrate the underlying mechanisms by which UC-MSCs cultured on decellularized ECM exhibited a stronger antioxidation against superoxide radicals, we evaluated two important antioxidative enzymes, SOD1 and SOD2, which catalyze superoxide radicals to hydrogen peroxide. Culturing of UC-MSCs on ECM upregulated *SOD1* mRNA expression by 25.0 ± 3.4% compared with the cells cultured on TCPS (Figure 4(A)); however, the difference of SOD1 protein levels between the two groups was not significant (Figure 4(B)). The *SOD2* mRNA level in ECM-cultured UC-MSCs was 2-fold higher (Figure 4(C)) and the protein expression was 40.2% higher (Figure 4(D)) than the cells on TCPS. Furthermore, SOD activity was increased by 70.0 ± 25.9% in UC-MSCs cultured on ECM compared with the cells cultured on TCPS (Figure 4(E)).

3.5 Effects of culturing UC-MSCs on ECM on H_2O_2-eliminating enzymes

Over-accumulation of H_2O_2 can cause oxidative damage to DNA, proteins, and lipids, and lead to cell death [26]. Therefore, we examined two important intracellular enzymes, catalase and GPx1, both of which catalyze the decomposition of hydrogen peroxide to water and oxygen. Culturing on ECM increased *CAT* mRNA expression in UC-MSCs by 17.6 ± 7.1% compared with the cells on TCPS (Figure 5(A)), but the protein levels were not significantly different (Figure 5(B)). The catalase activity of ECM-cultured UC-MSCs was 47.5 ± 9.8% higher than the TCPS-cultured cells (Figure 5(C)). With regard to GPx1, neither the mRNA expressions nor protein levels of the two groups were significantly different (Figure 5(D) and (E)).

3.6 Effects of culturing on ECM on H_2O_2-suppressed osteogenesis of UC-MSCs

The multi-lineage differentiation potentials of MSCs are important for their clinical applications; thus, UC-MSCs were cultured on TCPS and ECM separately, in osteogenic induction medium, with or without exogenous 100 μM H_2O_2 treatment, and the protective effects of culturing on ECM on MSC osteogenesis was analyzed. Cells incubated in growth medium served as a negative control. Alizarin Red S staining revealed mineralized matrix deposition during osteogenic differentiation, and no positive results were detected in the negative groups (Figure 6(A)). Quantitative analysis data showed that culturing on ECM induced a 2.2-fold increase of calcified matrix deposition compared with TCPS-cultured cells, and H_2O_2 treatment significantly decreased matrix mineralization (74.2 ± 3.3% reduction in the TCPS group and 15.2 ± 4.0% reduction in the ECM group, Figure 6(B)). We further evaluated transcript levels of osteoblast-specific genes using real-time RT-PCR. Culturing on ECM increased transcription of *COL1A1* by 2.4-fold and 6.6-fold compared to cells cultured on TCPS, with or without H_2O_2 treatment, respectively (Figure 6(C)). Expression of *SPP1* in ECM-cultured cells was 2.2-fold higher than TCPS-cultured cells with H_2O_2 treatment (Figure 6(D)). Similarly, the levels of *ALP* (Figure 6(E)), *RUNX2* (Figure 6(F)), *BGLAP* (Figure 6(G)), and *SP7* (Figure 6(H)) transcription were significantly elevated when cells were cultured on ECM with or without H_2O_2 treatment.

4. Discussion

MSCs have been widely used in research to develop cell-based therapeutic strategies for transplantation and tissue engineering; however, excessive levels of ROS in pathological conditions, probably caused by inflammatory cytokines, compromised the quality and survival of MSCs. For example, increased production of ROS was observed in chronic inflammation in osteoarthritis, leading to the impairment of the mitochondrial bioenergetic function and matrix catabolic processes in chondrocytes [27]. Thus, it is important to prevent oxidative stress-induced cell damage and improve cell survival in the process of *in vivo* transplantation. Our previous studies demonstrated MSCs cultured on decellularized ECM derived from synovium cells or bone marrow cells showed an attenuated level of ROS [17, 20]. It would be interesting to elucidate the underlying molecular mechanisms by which culturing on ECM modulated intracellular antioxidant defense in MSCs. The current study suggested that expression and activity of SOD2 and catalase were enhanced in MSCs cultured on ECM, resulting in the reduction of ROS and hydrogen peroxide.

There is accumulating evidence that ROS is indispensable for cell proliferation, lineage-specific differentiation, cell death, matrix homeostasis, and redox signaling mechanisms, but abnormal levels of ROS beyond cell tolerance resulted in irreversible damage to DNA, proteins, and lipids, followed by cellular senescence and cell death [28]. Our study found that culturing on ECM improved cell proliferation of UC-MSCs, accompanied by a higher percentage of cells in the S phase, when compared with cells cultured on TCPS. This finding may be because intracellular ROS in ECM-cultured MSCs decreased to a low-moderate level that facilitated cell growth [29]. Moreover, hydrogen peroxide is one of major components of ROS and plays a dual role in cell proliferation. It has been reported that low levels of H_2O_2 (< 10 μM) stimulated cell growth of fibroblasts, whereas cells exposed to high concentration of H_2O_2 (> 400 μM) underwent rapid apoptosis [30]. Our data showed that the level of intracellular H_2O_2 in ECM-cultured cells declined as well so that was possibly another important factor in supporting cell survival and fast expansion *in vitro*. In addition, the superoxide anion was proven to affect cell proliferation in a dose-dependent manner; low levels of superoxide anion stimulated cell proliferation, whereas it inhibited cell growth as the concentration increased [31]. Meanwhile, superoxide radicals other than H_2O_2 mediated the interleukin-1-induced signaling pathway that led to NF-κB activation in bovine articular chondrocytes [32]. Therefore, the effects of culturing on ECM on the intracellular superoxide anion in MSCs will be illustrated in future studies.

The most important findings in the present study are that expression and activity of intracellular antioxidative enzymes, in particular SOD2 and catalase, were superior in MSCs cultured on decellularized ECM than those cultured on TCPS. The enhancement of antioxidant capacity may explain the attenuation of ROS in UC-MSCs and benefit their therapeutic applications in pathological circumstances. An impaired activity of SOD2 in osteoarthritic chondrocytes was observed to not only cause oxidative damage to chondrocytes but also to promote the pathogenesis of osteoarthritis [33]. Therefore, treatments with exogenous antioxidants, such as melatonin, were applied to protect cells from oxidative stress by upregulating antioxidative enzymes [34]. Moreover, GPx1 was a critical enzyme that converts superoxide anion to H_2O_2. Although both the mRNA

and protein levels in ECM-cultured MSCs were comparable to those of TCPS-cultured cells, enhancement of GPx1 by selenium supplementation was demonstrated to reduce cell damage and improve cell proliferation [16].

Optimal stem cell growth and stemness characteristics are critical for MSC therapeutic potentiality; however, the microenvironment changes extensively from the *in vivo* niche to the *in vitro* uncoated TCPS surface. MSCs gradually lose their proliferative abilities and exhibit impaired multi-lineage differentiation potentials, which is attributed to a process of replicative senescence [35]. Consistent with the previous studies [17, 36, 37], our results demonstrated that culturing on ECM dramatically improved cell growth of MSCs, with retention of differentiation potential. Li et al. demonstrated that *in vitro* expansion of MSCs on ECM deposited by fetal cells was superior to ECM derived from adult cells [38]. More importantly, because the umbilical cord is an extraembryonic tissue, we assumed that ECM deposited by UC-MSCs would benefit *in vitro* expansion and further direct MSCs into lineage-specific commitment. UC-MSCs were isolated from the Wharton's jelly zone of the umbilical cord that was rich in abundant ECM proteins, such as collagen (Types I, III, IV, and VI), laminin, and heparan sulfate proteoglycans [39]. In agreement, our results revealed that, after decellularization, cell-deposited ECM consisted of multiple matrix proteins, and more importantly, retained the fibrous microstructure of nanoscale dimensions. Li et al. identified the composition of the decellularized ECM by proteomics analyses and showed that fibrillar collagens were the most abundant proteins including type I and III collagen [38]. Proteoglycans in the ECM have been shown to regulate cell adhesion, proliferation, and differentiation. Laminin, a proteoglycan with a large molecular weight, was identified in this study that supported lineage-specific differentiation of MSCs [40]. Small leucine-rich proteoglycans such as decorin, which contribute to matrix mineralization and collagen assembly during osteogenic differentiation [41], were confirmed by Lai et al. in the decellularized ECM [37]. However, the key bioactive components that contributes to cell proliferation are still unidentified. A recent study conducted by Lin et al. suggested that non-collagenous proteins in cell-deposited ECM, which could be extracted by urea, were the bioactive components supporting cell proliferation and migration [42]. In addition to protein components, the mechanical properties of culturing substrates, such as stiffness, have been reported to regulate lineage-specific differentiation of MSCs [43]. A downside to using the decellularized ECM as a culture system for MSCs is due to economical inefficiency; it costs more time and energy to generate the ECM and remove the precious cells. Therefore, our future work will focus on identifying the key bioactive components in the ECM and analyze the influence of matrix stiffness on MSC cell behavior. The bioactive components that are extracted from the decellularized ECM will be used to make the current TCPS culture system more efficient and economical.

The multi-lineage differentiation potentials of MSCs are important for their clinical applications. Our data demonstrated that continuous exposure to exogenous H_2O_2 suppressed MSC osteogenic differentiation, but culturing on ECM retained their differentiation capacity, as made evident by a higher level of matrix mineralization and osteoblast-specific marker gene expression. High doses of exogenously added H_2O_2 are toxic and compromise cell viability; to avoid the impact of different cell density on osteogenic differentiation, we chose a sublethal concentration of H_2O_2 at 100 μM, in

agreement with a previous report [44]. As shown in the images of Alizarin Red S staining, the cell density of MSCs was similar with or without H_2O_2 treatment, indicating that H_2O_2-induced inhibition of osteogenic differentiation was attributed to decreased differentiation capacity rather than compromised cell viability of UC-MSCs. Although the finding in this study is different from a previous report, in which treatment with H_2O_2 promoted osteogenic differentiation and calcification of vascular smooth muscle cells [45], we speculate that the controversial effects of H_2O_2 on osteogenic differentiation is dependent on specific cell types [46] and that MSCs derived from different sources exhibit different resistance to H_2O_2-induced oxidative stress [47].

The molecular mechanism by which culturing MSCs on ECM attenuated intracellular ROS accumulation and protected MSCs from H_2O_2-induced oxidative damage is not yet fully understood. Previous studies have demonstrated that SIRT1 is requisite for cell proliferation and defense against oxidative stress-induced senescence. Yuan et al. demonstrated that selective knockdown of SIRT1 resulted in a decline of cell growth of MSCs, but overexpression of SIRT1 restored the proliferation capacity [48]. Activation of SIRT1 prevented oxidative stress-induced apoptosis by upregulating catalase via the FoxO3a signaling pathway [49]. Our western blot analysis showed that protein levels of catalase were elevated in UC-MSCs cultured on ECM, which was associated with the enhanced antioxidant defense and attenuated intracellular levels of H_2O_2. In agreement with our findings, Li et al. observed that expression of SOD2 was increased by resveratrol (a SIRT1 agonist) treatment, but the promoting effects were reversed by SIRT1 inhibitor nicotinamide [50]. In addition, the protein p38 is involved in cell growth arrest, as evidenced by a previous study that demonstrated increased phosphorylation level of p38 contributed to H_2O_2-induced premature senescence in MSCs [51]. In this study, we found that phosphorylation of p38 was downregulated in ECM-cultured MSCs, suggesting that culturing on ECM might have anti-senescence effects to facilitate long-term *in vitro* expansion of MSCs. Further work is still necessary to elucidate the underlying mechanisms involving SIRT1 and p38 in ECM-cultured MSCs.

5. Conclusions

We conclude that the cellular response of UC-MSCs cultured on decellularized cell-deposited ECM showed attenuated intracellular ROS, enhanced antioxidative enzymes, and improved resistance to exogenous oxidative stress. Decellularized ECM can be an effective *in vitro* expansion system to produce sufficient amounts of MSCs and can potentially be an antioxidative treatment to prevent oxidative damage in transplanted MSCs. Future work will focus on identifying bioactive components, matrix mechanical properties of decellularized ECM, and investigating the underlying mechanism of the role of SIRT1 in ECM-cultured MSCs.

Acknowledgments

The authors are grateful to Suzanne Danley (West Virginia University, USA), Michelle Si (University of Waterloo, Canada), and Joseph Jargstorf (University of Waterloo, Canada) for carefully reviewing and editing the manuscript. This work was supported by the National Natural Science Foundation of China (No.51203194, No.31570978, No.51103182, No.31270995, No.81320108018); the National Institutes of Health (NIH) (R03 AR062763-01A1); Natural Science Foundation of Jiangsu Province (No.BK20140323); Jiangsu Provincial Special Program of Medical

Science (BL2012004); Jiangsu Provincial Clinical Orthopedic Center; the Priority Academic Program Development of Jiangsu Higher Education Institutions (PAPD); Scientific Research Foundation for the Returned Overseas Chinese Scholars, State Education Ministry; Science and Technology Program of Guangzhou [2013] 164, China.

References

[1]. Pittenger MF, et al. , Multilineage potential of adult human mesenchymal stem cells, Science 284 (5411) (1999) 143–147. [PubMed: 10102814]

[2]. Barry F, Murphy M, Mesenchymal stem cells in joint disease and repair, Nat. Rev. Rheumatol 9 (10) (2013) 584–594. [PubMed: 23881068]

[3]. Troyer DL, Weiss ML, Wharton's jelly-derived cells are a primitive stromal cell population, Stem Cells 26 (3) (2008) 591–599. [PubMed: 18065397]

[4]. Pappa KI, Anagnou NP, Novel sources of fetal stem cells: where do they fit on the developmental continuum?, Regen. Med 4 (3) (2009) 423–433. [PubMed: 19438317]

[5]. Corrao S, et al. , New frontiers in regenerative medicine in cardiology: the potential of Wharton's jelly mesenchymal stem cells, Curr. Stem Cell Res. Ther 8 (1) (2013) 39–45. [PubMed: 23278911]

[6]. Nagamura-Inoue T, He H, Umbilical cord-derived mesenchymal stem cells: Their advantages and potential clinical utility, World J. Stem Cells 6 (2) (2014) 195–202. [PubMed: 24772246]

[7]. Hsieh JY, et al. , Functional module analysis reveals differential osteogenic and stemness potentials in human mesenchymal stem cells from bone marrow and Wharton's jelly of umbilical cord, Stem Cells Dev. 19 (12) (2010) 1895–1910. [PubMed: 20367285]

[8]. Ho PJ, et al. , H2O2 accumulation mediates differentiation capacity alteration, but not proliferative decline, in senescent human fetal mesenchymal stem cells, Antioxid. Redox Signal 18 (15) (2013) 1895–1905. [PubMed: 23088254]

[9]. Bonnet CS, Walsh DA, Osteoarthritis, angiogenesis and inflammation, Rheumatology 44 (1) (2005) 7–16. [PubMed: 15292527]

[10]. Schiller J, et al. , Contribution of reactive oxygen species to cartilage degradation in rheumatic diseases: molecular pathways, diagnosis and potential therapeutic strategies, Curr. Med. Chem 10 (20) (2003) 2123–2145. [PubMed: 12871089]

[11]. Liu X, et al. , Melatonin mediates protective effects on inflammatory response induced by interleukin-1 beta in human mesenchymal stem cells, J. Pineal Res 55 (1) (2013) 14–25. [PubMed: 23488678]

[12]. Liu X, et al. , Rescue of proinflammatory cytokine-inhibited chondrogenesis by the antiarthritic effect of melatonin in synovium mesenchymal stem cells via suppression of reactive oxygen species and matrix metalloproteinases, Free Radic. Biol. Med 68 (2014) 234–246. [PubMed: 24374373]

[13]. Zelko IN, Mariani TJ, Folz RJ, Superoxide dismutase multigene family: a comparison of the CuZn-SOD (SOD1), Mn-SOD (SOD2), and EC-SOD (SOD3) gene structures, evolution, and expression, Free Radic. Biol. Med 33 (3) (2002) 337–349. [PubMed: 12126755]

[14]. Choi YJ, et al. , Cell-penetrating superoxide dismutase attenuates oxidative stress-induced senescence by regulating the p53-p21(Cip1) pathway and restores osteoblastic differentiation in human dental pulp stem cells, Int. J. Nanomedicine 7 (2012) 5091–5106. [PubMed: 23049256]

[15]. Mias C, et al. , Ex vivo pretreatment with melatonin improves survival, proangiogenic/mitogenic activity, and efficiency of mesenchymal stem cells injected into ischemic kidney, Stem Cells 26 (7) (2008) 1749–1757. [PubMed: 18467662]

[16]. Ebert R, et al. , Selenium supplementation restores the antioxidative capacity and prevents cell damage in bone marrow stromal cells in vitro, Stem Cells 24 (5) (2006) 1226–1235. [PubMed: 16424399]

[17]. He F, Chen X, Pei M, Reconstruction of an in vitro tissue-specific microenvironment to rejuvenate synovium-derived stem cells for cartilage tissue engineering, Tissue Eng. Part A 15 (12) (2009) 3809–3821. [PubMed: 19545204]

[18]. He H, et al. , Promotion of hepatic differentiation of bone marrow mesenchymal stem cells on decellularized cell-deposited extracellular matrix, Biomed Res. Int 2013 (2013) 406871. [PubMed: 23991414]

[19]. Bhat A, et al. , Differential growth factor adsorption to calvarial osteoblast-secreted extracellular matrices instructs osteoblastic behavior, PLoS One 6 (10) (2011) e25990. [PubMed: 21998741]

[20]. He F, et al. , Extracellular matrix modulates the biological effects of melatonin in mesenchymal stem cells, J. Endocrinol 223 (2) (2014) 167–180. [PubMed: 25210047]

[21]. Pei M, He F, Extracellular matrix deposited by synovium-derived stem cells delays replicative senescent chondrocyte dedifferentiation and enhances redifferentiation, J. Cell Physiol 227 (5) (2012) 2163–2174. [PubMed: 21792932]

[22]. He F, Pei M, Rejuvenation of nucleus pulposus cells using extracellular matrix deposited by synovium-derived stem cells, Spine 37 (6) (2012) 459–469. [PubMed: 21540772]

[23]. Pei M, et al. , Antioxidation of decellularized stem cell matrix promotes human synovium-derived stem cell-based chondrogenesis, Stem Cells Dev. 22 (6) (2013) 889–900. [PubMed: 23092115]

[24]. Rehan L, et al. , SIRT1 and NAD as regulators of ageing, Life Sci. 105 (1-2) (2014) 1–6. [PubMed: 24657895]

[25]. Debacq-Chainiaux F, et al. , p38(MAPK) in the senescence of human and murine fibroblasts, Adv. Exp. Med. Biol 694 (2010) 126–137. [PubMed: 20886761]

[26]. Veal EA, Day AM, Morgan BA, Hydrogen peroxide sensing and signaling, Mol. Cell 26 (1) (2007) 1–14. [PubMed: 17434122]

[27]. Liu-Bryan R, Terkeltaub R, Emerging regulators of the inflammatory process in osteoarthritis, Nat. Rev. Rheumatol 11 (1) (2015) 35–44. [PubMed: 25266449]

[28]. Chaudhari P, Ye Z, Jang YY, Roles of reactive oxygen species in the fate of stem cells, Antioxid. Redox Signal 20 (12) (2014) 1881–1890. [PubMed: 23066813]

[29]. Lewandowski D, et al. , In vivo cellular imaging pinpoints the role of reactive oxygen species in the early steps of adult hematopoietic reconstitution, Blood 115 (3) (2010) 443–452. [PubMed: 19797522]

[30]. Kim BY, Han MJ, Chung AS, Effects of reactive oxygen species on proliferation of Chinese hamster lung fibroblast (V79) cells, Free Radic. Biol. Med 30 (6) (2001) 686–698. [PubMed: 11295367]

[31]. Kang J, Zheng R, Dose-dependent regulation of superoxide anion on the proliferation, differentiation, apoptosis and necrosis of human hepatoma cells: the role of intracellular Ca 2+, Redox Rep. 9 (1) (2004) 37–48. [PubMed: 15035826]

[32]. Mendes AF, et al. , Differential roles of hydrogen peroxide and superoxide in mediating IL-1-induced NF-kappa B activation and iNOS expression in bovine articular chondrocytes, J. Cell. Biochem 88 (4) (2003) 783–793. [PubMed: 12577312]

[33]. Gavriilidis C, et al. , Mitochondrial dysfunction in osteoarthritis is associated with down-regulation of superoxide dismutase 2, Arthritis Rheum. 65 (4) (2013) 378–387. [PubMed: 23138846]

[34]. Fischer TW, et al. , Melatonin enhances antioxidative enzyme gene expression (CAT, GPx, SOD), prevents their UVR-induced depletion, and protects against the formation of DNA damage (8-hydroxy-2'-deoxyguanosine) in ex vivo human skin, J. Pineal Res 54 (3) (2013) 303–312. [PubMed: 23110400]

[35]. Wagner W, et al. , Replicative senescence of mesenchymal stem cells: a continuous and organized process, PLoS One 3 (5) (2008) e2213. [PubMed: 18493317]

[36]. Pei M, He F, Kish VL, Expansion on Extracellular Matrix Deposited by Human Bone Marrow Stromal Cells Facilitates Stem Cell Proliferation and Tissue-Specific Lineage Potential, Tissue Eng. Part A 17 (23-24) (2011) 3067–3076. [PubMed: 21740327]

[37]. Lai YL, et al. , Reconstitution of Marrow-Derived Extracellular Matrix Ex Vivo: A Robust Culture System for Expanding Large-Scale Highly Functional Human Mesenchymal Stem Cells, Stem Cells Dev. 19 (7) (2010) 1095–1107. [PubMed: 19737070]

[38]. Li J, et al. , Rejuvenation of chondrogenic potential in a young stem cell microenvironment, Biomaterials 35 (2) (2014) 642–653. [PubMed: 24148243]

[39]. Nanaev AK, et al. , Stromal differentiation and architecture of the human umbilical cord, Placenta 18 (1) (1997) 53–64. [PubMed: 9032810]

[40]. Lin HY, et al. , Fibronectin and laminin promote differentiation of human mesenchymal stem cells into insulin producing cells through activating Akt and ERK, J. Biomed. Sci 17 (2010) 56. [PubMed: 20624296]

[41]. Mochida Y, et al. , Decorin modulates collagen matrix assembly and mineralization, Matrix Biol. 28 (1) (2009) 44–52. [PubMed: 19049867]

[42]. Lin H, et al. , Influence of decellularized matrix derived from human mesenchymal stem cells on their proliferation, migration and multi-lineage differentiation potential, Biomaterials 33 (18) (2012) 4480–4489. [PubMed: 22459197]

[43]. Zhao W, et al. , Effects of substrate stiffness on adipogenic and osteogenic differentiation of human mesenchymal stem cells, Mater. Sci. Eng. C Mater. Biol. Appl 40 (2014) 316–323. [PubMed: 24857499]

[44]. Burova E, et al. , Sublethal oxidative stress induces the premature senescence of human mesenchymal stem cells derived from endometrium, Oxid. Med. Cell. Longev 2013 (2013) 474931. [PubMed: 24062878]

[45]. Byon CH, et al. , Oxidative stress induces vascular calcification through modulation of the osteogenic transcription factor Runx2 by AKT signaling, J. Biol. Chem 283 (22) (2008) 15319–15327. [PubMed: 18378684]

[46]. Lee DH, et al. , Effects of hydrogen peroxide (H2O2) on alkaline phosphatase activity and matrix mineralization of odontoblast and osteoblast cell lines, Cell Biol. Toxicol 22 (1) (2006) 39–46. [PubMed: 16463018]

[47]. Yoon SO, Yun CH, Chung AS, Dose effect of oxidative stress on signal transduction in aging, Mech. Ageing Dev 123 (12) (2002) 1597–1604. [PubMed: 12470897]

[48]. Yuan HF, et al. , SIRT1 is required for long-term growth of human mesenchymal stem cells, J. Mol. Med 90 (4) (2012) 389–400. [PubMed: 22038097]

[49]. Hasegawa K, et al. , Sirt1 protects against oxidative stress-induced renal tubular cell apoptosis by the bidirectional regulation of catalase expression, Biochem. Biophys. Res. Commun 372 (1) (2008) 51–56. [PubMed: 18485895]

[50]. Li YG, et al. , Resveratrol protects cardiomyocytes from oxidative stress through SIRT1 and mitochondrial biogenesis signaling pathways, Biochem. Biophys. Res. Commun 438 (2) (2013) 270–276. [PubMed: 23891692]

[51]. Zhou L, et al. , Melatonin reverses H_2O_2-induced premature senescence in mesenchymal stem cells via the SIRT1-dependent pathway, J. Pineal. Res 59 (2) (2015) 190–205. [PubMed: 25975679]

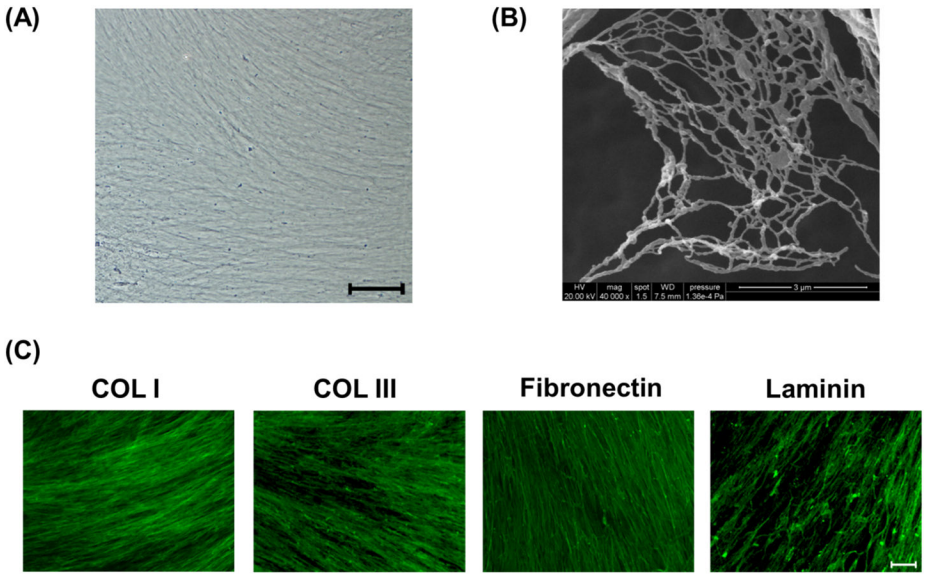

Fig.1.

Evaluation of decellularized extracellular matrix (ECM) deposited by UC-MSCs. (A) Decellularized ECM showed a fibrous structure in a representative bright field image. Scale bar = 100 μm. (B) Scanning electron microscopy analysis revealed that decellularized ECM was composed of net-like lattices with small bundles of collagen fibers. Scale bar = 3 μm. (C) Representative images of immunofluorescence staining identified four matrix proteins (type I and III collagens, fibronectin, and laminin) in decellularized ECM. Scale bar = 100 μm.

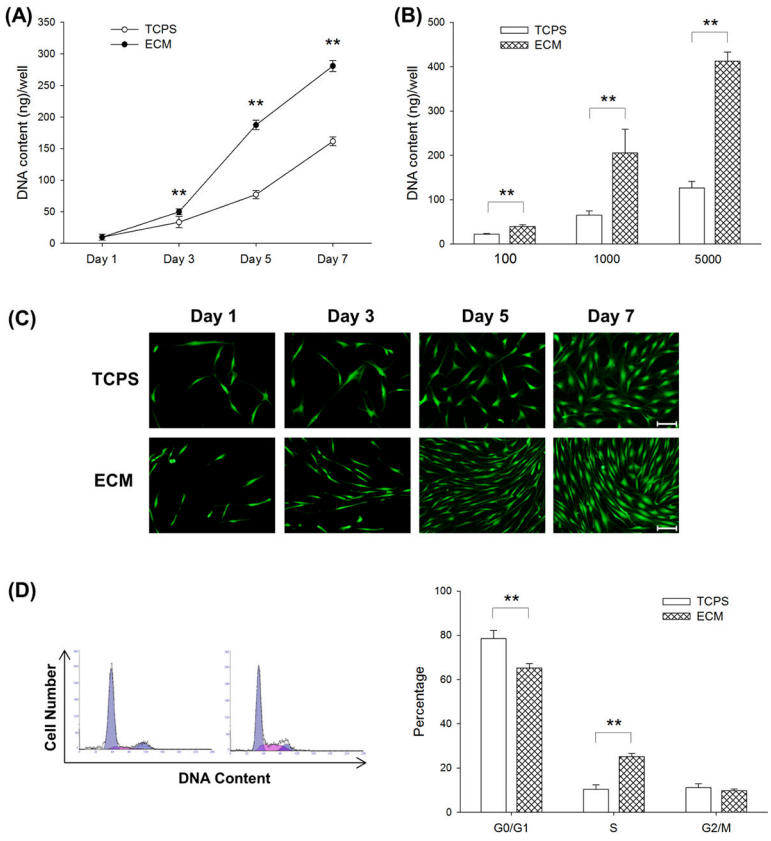

Fig.2.

Effects of culturing on ECM on cell proliferation and cell cycle phase distribution in UC-MSCs. (A) UC-MSCs were seeded on TCPS and ECM-coated surfaces at the cell density of 1,000 cells/cm^2. The DNA content, representing cell proliferation, was assessed on days 3, 5, and 7. (B) UC-MSCs were seeded on TCPS and ECM at the cell density of 100, 1,000, and 5,000 cells/cm^2. The DNA content was assessed on day 5. (C) Cell morphology and density were observed in representative fluorescence images labeled by fluorescein diacetate (FDA) when UC-MSCs were initially cultured at the cell density of 1,000 cells/cm^2. Scale bar = 100 μm. (D) The cell cycle phase distribution of UC-MSCs cultured on TCPS and ECM was measured by flow cytometry analysis. Values are the mean ± S.E. of five independent experiments (n = 5) in the DNA content assay and of three independent experiments (n = 3) in the cell cycle phase distribution analysis. Statistically significant differences are indicated by ** ($p < 0.01$). TCPS: tissue culture polystyrene; ECM: extracellular matrix.

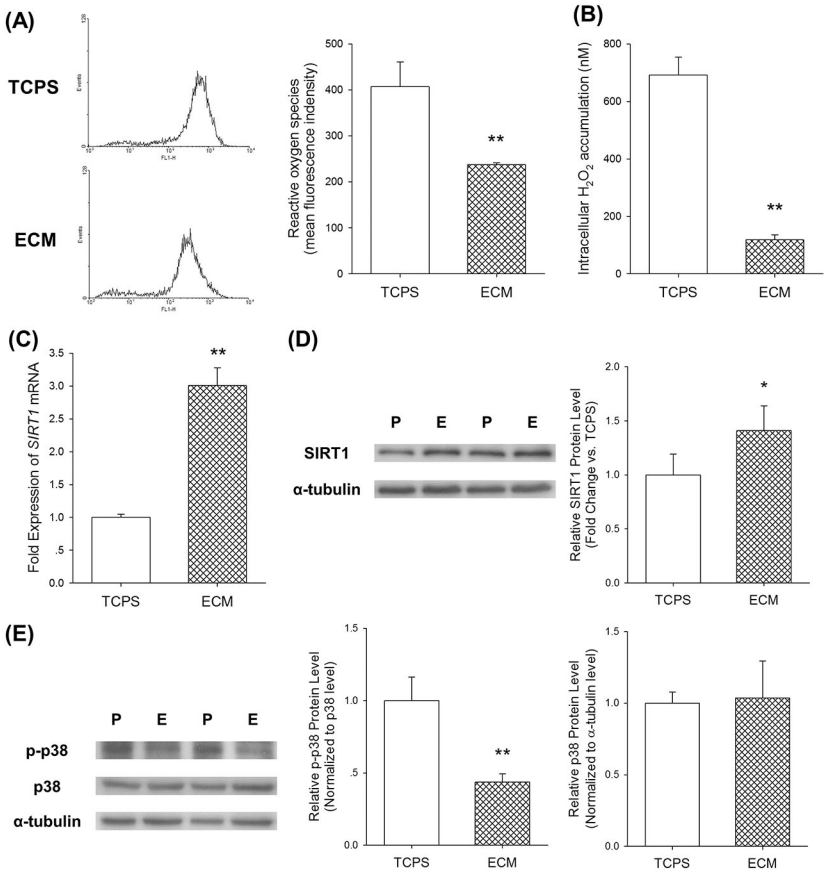

Fig.3.

Culturing on ECM attenuated accumulation of intracellular reactive oxygen species (ROS). (A) Intracellular ROS of UC-MSCs cultured on TCPS and ECM was labeled by DCF-DA and fluorescence intensity was measured by flow cytometry. (B) Intracellular hydrogen peroxide of UC-MSCs cultured on TCPS and ECM was labeled by Amplex® Red dye. (C) The mRNA level of *SIRT1* was measured by real-time RT-PCR. (D) Culturing on ECM upregulated the protein level of SIRT1, determined by western blot analysis. The α-tubulin lane served as a loading control. (E) Culturing on ECM downregulated phosphorylation (p-) of p38 MAPK. The level of p-p38 was normalized to total p38 protein. The level of p38 was normalized to the α-tubulin protein. Values are the mean ± S.E. of four independent experiments (n = 4) in ROS analysis, hydrogen peroxide analysis, real-time RT-PCR, and western blot analysis. Statistically significant differences are indicated by * ($p < 0.05$) or ** ($p < 0.01$). P: TCPS/ tissue culture polystyrene; E: ECM/extracellular matrix.

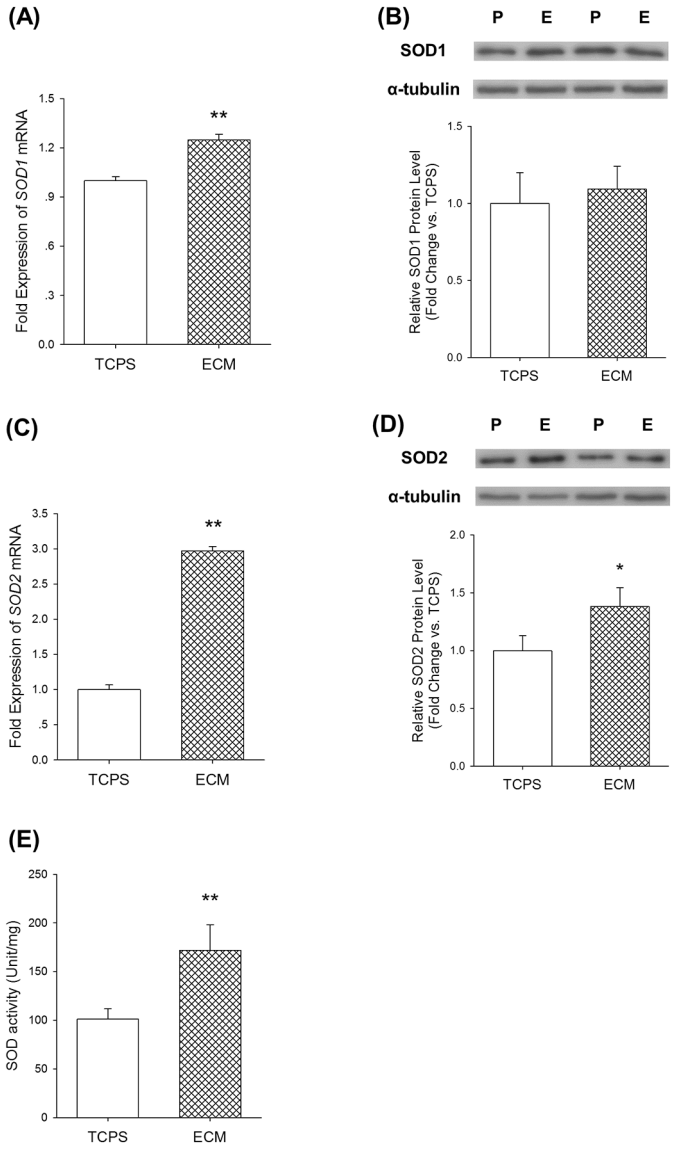

Fig.4.

Effects of culturing on ECM on superoxide dismutase (SOD) in UC-MSCs. (A) Culturing on ECM upregulated *SOD1* mRNA expression in UC-MSCs, determined by real-time RT-PCR. (B) The protein levels of SOD1, measured by western blot analysis, did not change in cells cultured on TCPS and ECM. (C) Culturing on ECM increased *SOD2* mRNA expression in UC-MSCs. (D) The protein level of SOD2 was enhanced in ECM-cultured UC-MSCs. (E) Culturing on ECM improved SOD activity in UC-MSCs. Values are the mean ± S.E. of four independent experiments (n = 4) in real-time RT-PCR, western blot analysis, and SOD activity analysis. Statistically significant differences are indicated by * ($p < 0.05$) or ** ($p < 0.01$). P: TCPS/ tissue culture polystyrene; E: ECM/extracellular matrix.

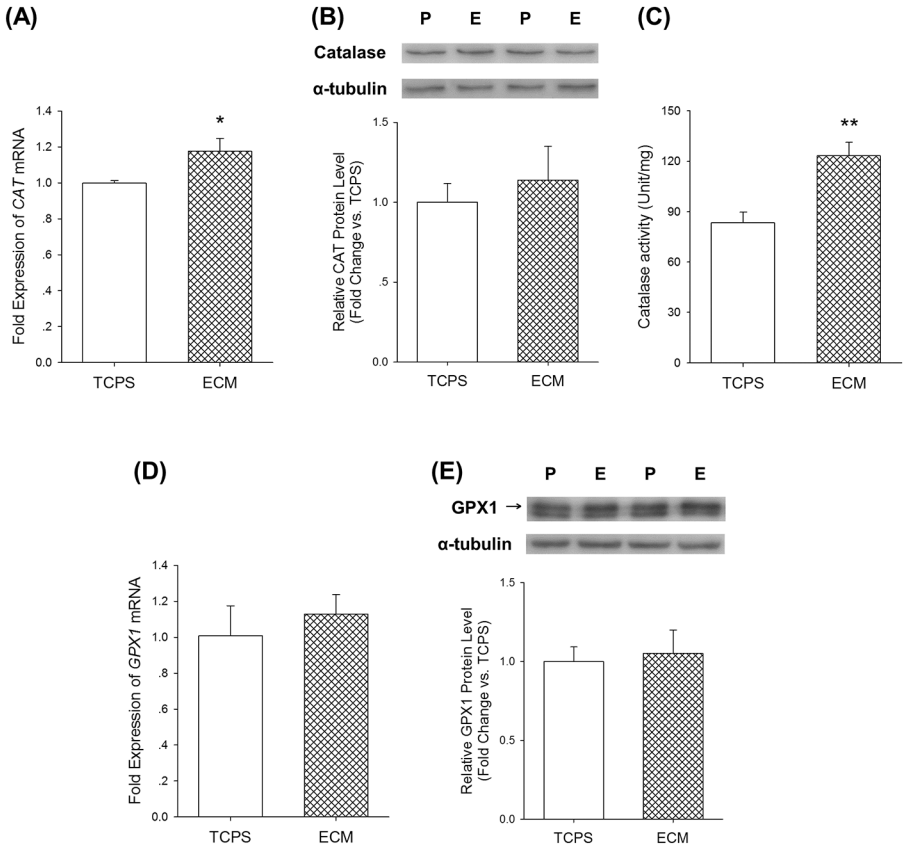

Fig.5.

Effects of culturing on ECM on catalase and GPx1 in UC-MSCs. (A) Culturing on ECM upregulated *CAT* mRNA expression in UC-MSCs, determined by real-time RT-PCR. (B) The protein levels of catalase, measured by western blot analysis, did not change in cells cultured on TCPS and ECM. (C) Culturing on ECM improved catalase activity in UC-MSCs. (D) The mRNA level of *GPX1* did not change in ECM-cultured cells. (E) The protein level of GPx1 did not change in ECM-cultured cells. Values are the mean ± S.E. of four independent experiments (n = 4) in real-time RT-PCR, western blot analysis, and catalase activity analysis. Statistically significant differences are indicated by * ($p < 0.05$) or ** ($p < 0.01$). P: TCPS/ tissue culture polystyrene; E: ECM/extracellular matrix.

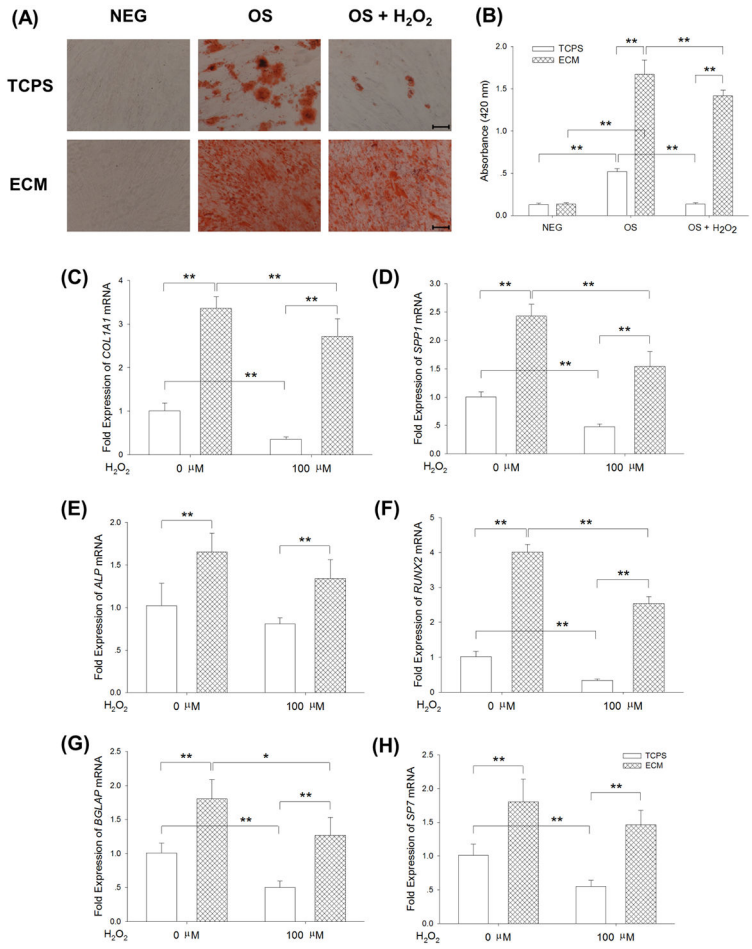

Fig.6.

Culturing on ECM improved resistance of UC-MSCs to exogenous H_2O_2 and restored the osteogenic differentiation capacity. UC-MSCs were cultured on TCPS and ECM, and continuously treated with 100 μM H_2O_2 during osteogenic differentiation. (A) Representative images of Alizarin Red S staining, indicating mineralization of the matrix, showed that treatment with H_2O_2 suppressed matrix calcification in TCPS-cultured cells, but culturing on ECM retained the capacity of UC-MSCs for calcified matrix deposition. (B) The stained mineral layers were dissolved in 1% hydrochloric acid and were quantified via a spectrophotometer. (C)-(H) The mRNA levels of osteoblast-specific marker genes, including *COL1A1* (C), *SPP1* (D), *ALP* (E), *RUNX2* (F), *BGLAP* (G), and *SP7* (H) were measured by real-time RT-PCR. Values are the mean ± S.E. of four independent experiments (n = 4) in Alizarin Red S staining and real-time RT-PCR. Statistically significant differences are indicated by * ($p < 0.05$) or ** ($p < 0.01$). TCPS: tissue culture polystyrene; ECM: extracellular matrix; NEG: negative control; OS: osteogenic induction; H_2O_2: hydrogen peroxide.

Table 1.

Primers used for Real-time RT-PCR

Gene	Forward Primer sequence(5'-3')	Reverse Primer sequence(5'-3')
GAPDH	AGAAAAACCTGCCAAATATGATGAC	TGGGTGTCGCTGTTGAAGTC
SIRT1	GCGGGAATCCAAAGGATAAT	CTGTTGCAAAGGAACCATGA
SOD1	GGTGGGCCAAAGGATGAAGAG	CCACAAGCCAAACGACTTCC
SOD2	GGGGATTGATGTGTGGGAGCACG	AGACAGGACGTTATCTTGCTGGGA
CAT	TGGGATCTCGTTGGAAATAACAC	TCAGGACGTAGGCTCCAGAAG
GPX1	TATCGAGAATGTGGCGTCCC	TCTTGGCGTTCTCCTGATGC
COL1A1	CAGCCGCTTCACCTACAGC	TTTTGTATTCAATCACTGTCTTGCC
SPP1	GCGAGGAGTTGAATGGTG	CTTGTGGCTGTGGGTTTC
ALP	AGCACTCCCACTTCATCTGGAA	GAGACCCAATAGGTAGTCCACATTG
RUNX2	AGAAGGCACAGACAGAAGCTTGA	AGGAATGCGCCCTAAATCACT
BGLAP	GAGCCCCAGTCCCCTACC	GACACCCTAGACCGGGCCGT
SP7	CACTCACACCCGGGAGAAGA	GGTGGTCGCTTCGGGTAAA